Investigating the abnormal conductivity behaviour of divalent cations in low dielectric constant tetraglyme-based electrolytes

Long Hoang Nguyen, Tanguy Picard, Cristina Iojoiu, Fannie Alloin, Nicolas Sergent, Marie Liesse Doublet, Jean-Sébastien Filhol

ARTICLE

Investigating the Abnormal Conductivity Behaviour of Divalent Cations in Low Dielectric Constant Tetraglyme-Based Electrolytes

Received 00th January 20xx,
Accepted 00th January 20xx

DOI: 10.1039/x0xx00000x

Long Hoang Bao Nguyen,[a#] Tanguy Picard,[b#] Cristina Iojoiu,[b,c]* Fannie Alloin,[b,c] Nicolas Sergent,[b] Marie-Liesse Doublet [a,d]* and Jean-Sébastien Filhol [a,d]*

Solutions made of tetraglyme (G4) containing $Ca(TFSI)_2$ have been studied as models to understand the solvation structure and the conductivity properties of multivalent ions in low dielectric constant ethereal electrolytes. These solutions have been characterised using electrochemical impedance spectroscopy, rheological measurement, and Raman spectroscopy. The ionic conductivity of such electrolytes shows an intriguing non-monotonic behaviour with temperature which deviates from the semi-empirical Vogel-Tamman-Fulcher equation at a critical temperature. This behaviour is observed for both $Mg(TFSI)_2$ and $Ca(TFSI)_2$, but not LiTFSI, indicating a difference in the solvation structure and the thermodynamic properties of divalent ions compared to Li^+. The origin of this peculiar behaviour is demystified using temperature-controlled Raman spectroscopy and first-principles calculations combined with a thermodynamic analysis of the chemical equilibrium of Ca^{2+} ion-pairing versus solvation. As long-range electrostatic interactions are critical in solutions based on low dielectric ethereal solvents, a periodic approach is here proposed to capture their impact on the solvation structure of the electrolyte at different salt concentrations. The obtained results reveal that the thermodynamic and transport properties of $Ca(TFSI)_2$/G4 solutions stem from a competition between enthalpic (ionic strength) and entropic factors that are directly controlled by the solution concentration and temperature, respectively. At high salt concentrations, the ionic strength of the solution favours the existence of free ions thanks to the strong solvation energy of the polydentate G4 solvent conjugated with the weak complexation ability of TFSI-. At elevated temperatures, the configurational entropy associated with the release of a coordinated G4 favours the formation of contact ion-pair due to its flat potential energy surface (weak strain energy), offering a large configuration space. Such a balance between ion-pair association and dissociation not only rationalises the ionic conductivity behaviour observed for $Ca(TFSI)_2$/G4 solutions but also provides valuable information to extrapolate the ionic transport properties of other electrolytes with different $M(TFSI)_n$ salts dissolved in longer-chain glymes or even poly(ethylene oxide). These findings are essential for the understanding of solvation structures and ionic transport in low-dielectric media, which can further be used to design new electrolytes for Li-ion and post Li-ion batteries as well as electrocatalysts.

Introduction

Global battery market has been in constant expansion in recent years with tremendous development is foreseen in the next decades as induced by the immediate consequence of electrified transportation and the installation of electrical grid storage to accommodate the intermittent energy production. In order to ensure a sustainable supply chain, battery productions need to be "green" regarding their environmental impact.[1,2] So far, rechargeable lithium-ion batteries (LIBs) are the dominant energy storage technology for mobile devices, but lithium mining has caused significant ecological and social effects.[3,4] Furthermore, the use of rare metals such as cobalt in these batteries has caused great impacts on the environment and the price of the full device.[5] Academic and industrial research nowadays aim to minimise the use of rare metals in batteries, and improve the power and energy densities of the cells. In order to ensure an ecological and sustainable supply of batteries adapted to our modern life's demands, calcium-ion rechargeable batteries have been explored.[6–9] Indeed, Ca is the fifth most abundant element on Earth, available in most countries at a reasonable extraction price, by-passing all the economic and political constraints in the technological transition to come. Furthermore, calcium is safer than lithium due to its lower reactivity when exposed to air and moisture.

The growth of calcium-ion rechargeable batteries is conjugated to the development of new Ca^{2+}-conducting electrolytes. In order to satisfy all the practical requirements, the newly developed electrolyte must possess a high Ca^{2+} conductivity (>10^{-4} S·cm^{-1} at room temperature), a transference number of Ca^{2+} approaching 1, and high chemical and electrochemical stabilities.[10,11] Moreover, materials used as electrolyte must be safe, non-flammable, having

[a.] *ICGM, Univ Montpellier, CNRS, ENSCM, Montpellier, France.*
[b.] *Univ. Grenoble Alpes, Univ. Savoie Mont Blanc, CNRS, Grenoble INP, LEPMI, 38000 Grenoble, France.*
[c.] *RS2E French Network on Electrochemical Energy Storage, FR5439, Amiens, France*
[#] Authors contributed equally.
†Electronic Supplementary Information (ESI) available. See DOI: 10.1039/x0xx00000x

low toxicity and low manufacturing cost. Organic carbonates have long been used as solvents for electrolytes in LIBs thanks to their high dielectric constant, wide electrochemical windows, and the capability to dissolve a considerable amount of salts at ambient temperature.[12] Nonetheless, recent research has shown that carbonate-based electrolytes are not ideal for multivalent batteries as the solvent molecules tend to be reduced before the metal deposition can occur.[13] Promising Ca plating and stripping have recently been reported in electrolytes using glyme- or ether-based solvents, indicating the particular role of low dielectric media in the electrochemical activity of multivalent ions.[14–17]

To design proficient Ca^{2+} electrolytes, the solvation structure, the physical properties, and the conduction mechanism in Ca^{2+} electrolytes should be well comprehended. Among the glyme-based family, tetraethylene glycol dimethyl ether (tetraglyme or G4), exhibits intermediate properties between molecular and polymer glymes. A detailed investigation of Ca^{2+}–O interaction tetraglyme solution is thus representative for the whole glyme family. Most glyme molecules possess a high donor number (DN), which is a measure of the Lewis basicity of the oxygen's electron lone pairs, helping them to dissolve a significant amount of Ca^{2+} salts. Nevertheless, glyme-based solvents possess a low dielectric constant (ε_r = 7.0–7.5), leading to great complexities when examining their physical properties. When dissolved in solution, a solvated ion can still interact with other cations and anions through the long-range electrostatic interaction, whose energy can be expressed by $U = \frac{q_1 q_2 e^2}{4\pi\varepsilon_0\varepsilon_r r}$ with r being the distance between the two ions of charge q_1 and q_2 that are present in a medium of ε_r dielectric constant. In conventional carbonate-based electrolytes, the dielectric constant is high (ε_r = 89.0 for ethylene carbonate or ε_r = 40–60 for mixtures of carbonated solvents) so that the ion–ion interactions are efficiently screened by the solvents, which significantly reduces their contribution to the system's total energy. Whereas the ionic interactions can be reasonably estimated by the Debye-Hückel theory[18], it is only applicable to diluted solutions (~ 0.01–0.1 M) in high-dielectric media and cannot be universally applied. In order to model and predict the thermodynamic properties of low-dielectric media in a qualitative way, it is necessary to develop a new modelling approach to account for the contribution of these long-range electrostatic interactions.

In this study, several $Ca(TFSI)_2$/G4 solutions were prepared, and their ionic conductivity and viscosity were evaluated at different temperatures and concentration, then compared with LiTFSI/G4 electrolyte. Abnormal behaviours were detected in $Ca(TFSI)_2$/G4 solutions and the origin of these abnormalities was thoroughly investigated using a combined experimental and theoretical approach. In these solutions, contact ion-pairs occur preferentially at elevated temperatures, and differs from those usually observed in Li^+ electrolytes. The ion-pair structure was elucidated using first-principles Density Functional Theory (DFT) calculations combined with vibrational spectroscopy. Furthermore, the chemical equilibrium between ion-pair association and dissociation was estimated by periodic calculations to include the effect of the long-range electrostatic interactions on the energy of the charged ions at different salt concentrations. The obtained results reveal that the ion-pair formation is an endergonic process that turns to be exergonic at high temperatures or low salt concentrations due to a subtle balance between the ionic strength of low-dielectric media and entropy gain when G4 molecules are released during the ion-pairing. Such a fundamental knowledge in ion-pair formation mechanism is vital to the understanding of solvation properties in low-dielectric media, which is not fully comprehended at the present time. Moreover, the results discovered in this work can be used as guidance to develop new electrolytes for rechargeable batteries, especially those using non-polar solvents.

Results

Conductivity and Viscosity Measurements. The conductivity (σ) of $Ca(TFSI)_2$/G4 solutions was measured at different salt concentrations in a temperature range of -20 to 90°C (**Figure 1a**). By varying the salt concentration, the ionic conductivity of $Ca(TFSI)_2$/G4 solutions increases monotonically up to 0.7 M while in the case of $Mg(TFSI)_2$/G4 the conductivity maxima was observed at 0.55 M.[19] The reason for this difference is related to the solvation structure of Mg^{2+}/Ca^{2+} in G4 and the energy of the M^{2+}–O interaction. The measured conductivity was then fit using the semi-empirical Vogel–Tammann–Fulcher (VTF) model (Equation (1)), which generally describes the conductivity behaviour of amorphous polymer and liquid electrolytes *vs* temperature.

$$\sigma = \frac{\sigma_0}{\sqrt{T}} * exp\left(\frac{-B}{R(T-T_0)}\right) \qquad \text{Equation (1)}$$

σ is the ionic conductivity of the solution, the pre-factor σ_0 characterises the inherent conductivity of the electrolyte and is related to charge carrier concentration and attempt frequency for ions to transit between solvation sites. B is a constant representing the pseudo-activation energy related to the segmental motion of the polymer/solution. T_0 is the Vogel temperature, commonly called ideal glass transition temperature, below which no more segmental motion is possible. It is generally observed that $T_0 \approx \frac{3}{4}T_g \approx \frac{1}{2}T_m$ (with T_g the glass transition temperature and T_m the melting temperature) for polymer-based electrolytes.[20–22]

A severe deviation from the VTF model is observed at a relatively low temperature for all solutions, e.g. 37°C for 0.5 M $Ca(TFSI)_2$/G4 solution (**Figure 1b**). This behaviour is abnormal as in typical solutions, charge carriers' mobility increases with temperature due to the viscosity decreases. Furthermore, the "critical temperature" (T_c) associated with the onset of the deviation from the VTF law, shifts to a lower temperature when lowering the salt concentration, from T_c = 333 K in 0.8 M $Ca(TFSI)_2$/G4 to 293 K in 0.1 M solution. Such a deviation is not observed in 0.5 M LiTFSI/G4 solution (**Figure S2**) and has never been reported to the best of our knowledge. The presence of a "critical temperature" in $Ca(TFSI)_2$/G4 electrolytes could be a consequence of the low dielectric constant value of G4 that strongly increases long-range cation/anion electrostatic interactions, in particular for solutions based on divalent cations. Forero-Saboya *et al*. investigated carbonate-based electrolytes and also observed a different behaviour for Mg^{2+} or Ca^{2+}-based electrolytes compared to Li^+ one; nevertheless, the evolution in the conductivity of these carbonate-based electrolytes followed the VTF model, even at high temperatures.[23]

The temperature dependence of the viscosity of $Ca(TFSI)_2$/G4 solutions at different salt concentrations is depicted in **Figure 1c**. The addition of $Ca(TFSI)_2$ into liquid tetraglyme led to an increase in the solution viscosity as a consequence of the interaction between Ca^{2+} and the G4 electron lone-pairs. By increasing temperature, the viscosity drops rapidly, and its evolution *vs* temperature follows the

VTF model perfectly, which is not the case for conductivity. At a given temperature, the conductivity increases continuously with the concentration while a discontinuity is noticed for the viscosity, i.e. a large increase in the solution viscosity is observed when moving from 0.6 M to 0.7 M solution. This viscosity/conductivity non-correlated process could be related to the formation of a gel due to Ca^{2+}–O interactions at a certain concentration. However, such a structure was not observed by rheology measurements showing that $Ca(TFSI)_2$/G4 electrolytes behave as a Newtonian liquid irrespectively of the salt concentration (**Figure S3**). DSC measurements were also performed (**Figure S4**) and contrarily to what has been observed for lithium electrolytes in G4,[24,25] two melting points were observed up to 0.8 M, indicating the presence of crystalline solvate structures with a low melting point at around -32°C. The eutectic point corresponds to the 0.8 M concentration, i.e. a molar ratio of four G4 per $Ca(TFSI)_2$.

To further investigate the link between conductivity and viscosity, one can plot their product, normalised by the salt concentration, as a function of temperature (**Figure 1d**), known as the Walden plot $\frac{S*\eta}{C} = f(T)$ [26,27]. In a liquid or amorphous polymer, the ionic conductivity is linked to the motion of both anions and cations, and the charge mobility is in turn linked to the ability of the host network to accommodate the charge transport, which is quantified by its viscosity and structural relaxation time. In general cases, the viscosity and conductivity are inversely proportional, making their normalised product a constant with respect to temperature, which is the case of 0.5 M LiTFSI/G4 (**Figure 1d**). Nevertheless, the constant line in the Walden plot only holds in solutions, where the number of charge carriers is constant in the investigating temperature range. In 0.1–0.3 M $Ca(TFSI)_2$/G4 solutions, the Walden plot shows a plateau at low temperature, followed by a slight deviation at higher temperatures. On the other hand, the Walden plot deviates brutally from the constant line in 0.4–0.8 M $Ca(TFSI)_2$/G4 solutions, which might be related to a change in the number and/or the nature of charger carriers with temperature (**Figure 1d**). This behaviour has been previously reported for $Ca(NO_3)_2$ hydrate melts, and this abnormality was assigned to structures formed in the liquid phase.[28]

Origin of abnormal behaviours. The deviation in the conductivity and the Walden plots of $Ca(TFSI)_2$/G4 solutions indicates a decrease in the number of charge carriers and the formation of new ionic species in the solution at elevated temperatures. One possibility for the change in the number of charge carriers is the ion-pair formation. Nevertheless, the actual structure of $[Ca–TFSI]^+$ contact ion-pair in G4 solution has never been reported in the literature. Theoretical DFT calculations were thus employed to elucidate the structure and shed light on the mechanism of the ion-pairing.

In a recent work, we reported that Ca^{2+} ions in 0.5 M $Ca(TFSI)_2$/G4 solution is solvated mainly in the form of *mer*-$[Ca(G4)_2]^{2+}$, in which two G4 molecules participate in the solvation, each G4 donating four of its oxygens to the coordination to Ca^{2+}, i.e. [4+4].[29] The complexation to $TFSI^-$ requires the departure of one G4 molecule in *mer*-$[Ca(G4)_2]^{2+}$ and leads to a [5+2] solvation sphere in which one Ca–O bond is missing compared to the fully solvated [4+4] sphere (**Figure 2**). In $TFSI^-$, the negative charge is delocalised over O=S–N–S=O group, in which both N and O atoms can act as electron donors. Experimental and theoretical data have shown that oxygens in sulfonyl groups have a higher affinity to cations than nitrogen in the imide.[30–34] Furthermore, the nitrogen atom has a great steric hindrance in its surrounding; hence, only oxygens participate in the ion-pair formation. Different conformations and structures of $TFSI^-$ and $[Ca(TFSI)(G4)]^+$ contact ion-pair were generated and discussed in **Figures S5** and **S6**. Results show that *trans*-$[Ca(\mu_2\text{-}TFSI)(G4)]^+$ is the most stable form, contributing mainly to the thermodynamic properties of the solutions, which will be focused in the following parts.

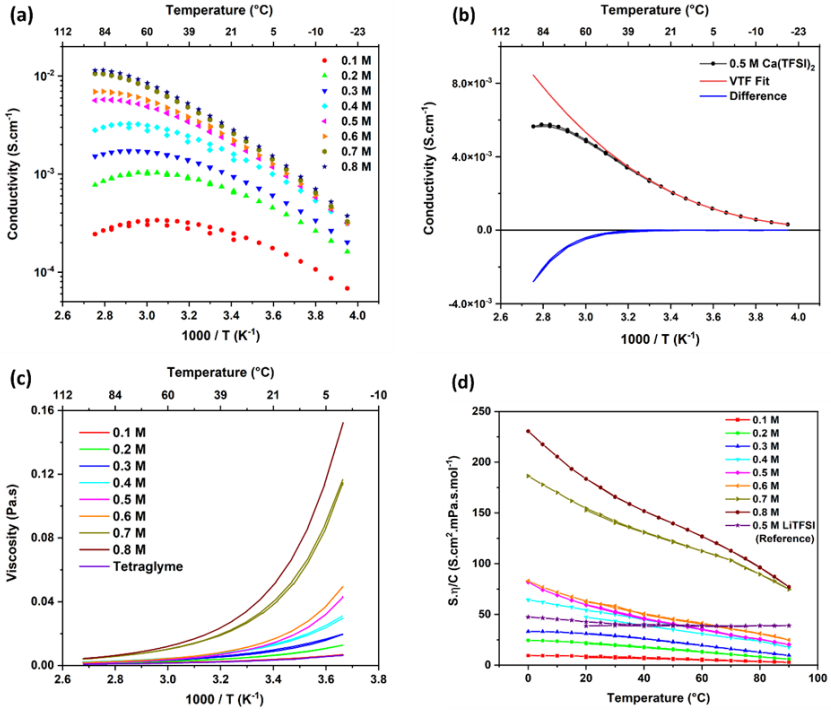

Figure 1. (a) Temperature dependence of the conductivity of $Ca(TFSI)_2$/G4 solutions at different salt concentrations. (b) VTF fit of the conductivity recorded on a 0.5 M $Ca(TFSI)_2$/G4 solution. (c) Temperature dependence of the viscosity of $Ca(TFSI)_2$/G4 solutions at different

salt concentrations. (d) Walden plot of $Ca(TFSI)_2$/G4 solutions at different salt concentrations. The Walden plot of a 0.5 M LiTFSI/G4 solution was plotted as a reference for comparison purposes.

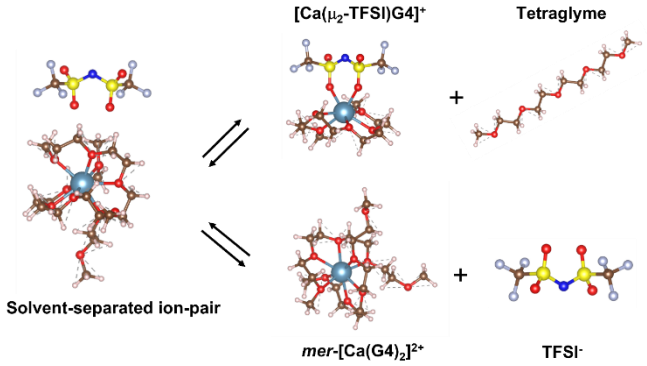

Figure 2. Molecular representation of $[mer\text{-}[Ca(G4)_2]//TFSI]^+$ solvent-separated ion-pair and its evolution to $trans\text{-}[Ca(\mu_2\text{-}TFSI)(G4)]^+$ contacting ion-pair and free ions.

Due to its high charge value, *mer*-$[Ca(G4)_2]^{2+}$ complex can attract and interact with free $TFSI^-$ in the solution to form the solvent-separated ion-pair $[[Ca(G4)_2]//TFSI]^+$. In this structure, Ca^{2+} remains fully bonded to G4 molecules while $TFSI^-$ resides in its second solvation shell in a relatively close distance (**Figure S7**). Even though $TFSI^-$ is not directly bonded to the Ca^{2+} centre, the electrostatic interaction between them limits the free motion of the ions, thus having a direct impact on the solution's ionic conductivity. Due to the mechanical flexibility of long tetraglyme chains, $[Ca(G4)_2]^{2+}$ can adopt several solvation structures with different organisations of tetraglyme molecules. Instead of having a [4+4] coordination as in the *mer*-structure, $[Ca(G4)_2]^{2+}$ can adopt a [5+3] solvation sphere (**Figure S8**), where the energy difference between the two forms is only 37.7 $kJ{\cdot}mol^{-1}$ (390 meV)[29], which is accessible by a gain in the configurational entropy of the less coordinated G4 molecule or thermal excitation. By considering different conformers, the energy of $[[Ca(G4)_2]//TFSI]^+$ solvent-separated ion-pair can then span over an energy range of 37.7 $kJ{\cdot}mol^{-1}$ depending on the local configuration of the coordinated G4 molecules (**Figure 3**), such energy span is also expected for free ions. In reality, the energy of $[[Ca(G4)_2]//TFSI]^+$ solvent-separated ion-pair spans over a wider than free ions due to (i) different conformers of solvated Ca^{2+}, (ii) the distance between solvated Ca^{2+} and $TFSI^-$, and (iii) the direction where $TFSI^-$ approaches the solvated Ca^{2+}. Nonetheless, all these factors cannot fully be captured due to the limitations of DFT calculations, we have thus limited our consideration in the conformer contribution.

The total energy of different Ca^{2+} solvation and ion-pair structures as a function of the solution concentration is reported in **Figure 3**. The results show that $[[Ca(G4)_2]//TFSI]^+$ solvent-separated ion-pair is the most stable species, especially at low concentrations (**Figure 3**). This result agrees with previous studies showing that multivalent ions were prone to ion-pairing even at modest concentrations.[35–39] This emphasises that even though G4 is capable of dissolving $Ca(TFSI)_2$ salt thanks to the strong Ca^{2+}–O interaction (see **Table 1**), the solvated $[Ca(G4)_2]^{2+}$ are not completely separated from $TFSI^-$. The strong electrostatic interactions of Ca^{2+} with its surroundings thus make the motion and properties of solvated Ca^{2+} strongly correlated with its counter-ions at all concentrations.

The energy of doubly-charged *mer*-$[Ca(G4)_2]^{2+}$ is more sensitive to the solution concentration than the singly-charged solvent separated $[[Ca(G4)_2]//TFSI]^+$ and contact ion-pair *trans*-$[Ca(\mu_2\text{-}TFSI)(G4)]^+$. Consequently, the fully solvated species becomes more stable than the solvent-separated and contact ion-pair species at a critical concentration above which higher molar fraction of *mer*-$[Ca(G4)_2]^{2+}$ should occur in the solution. This leads to the existence of three distinct regions in the phase diagram (**Figure 3**), in which the thermodynamic stability of the solvated species is ranked as follows:

- Region 1 (Low concentration): Solvent-separated ion-pair > Contact ion-pair > Free ions.
- Region 2 (Medium concentration): Solvent-separated ion-pair > Free ions > Contact ion-pair.
- Region 3 (High concentration): Free ions > Solvent-separated ion-pair > Contact ion-pair.

Interestingly, the conversion of the most stable species, i.e. solvent-separated ion-pairs or free ions, to contact ion-pairs is computed as an endergonic process (~100–200 meV) at 0 K. As this process is accompanied with a release of a tetraglyme molecule which possesses high configurational entropy due to the long organic chain with several degrees of freedom associated with the rotations around the chemical C–O, C–C bonds, the chemical equilibrium should turn in favour of the ion pair formation at elevated temperatures due to significant entropy gain. Indeed, the energy difference between solvent-separated ion-pairs/free ions and contact ion-pairs is around 100 meV (**Figure 3**), which can be easily compensated by vibrational and configurational entropy contributions of free tetraglyme molecules at elevated temperatures. Upon heating, it is therefore expected that $[Ca(\mu_2\text{-}TFSI)(G4)]^+$ contact ion-pair formation can occurs, which can alter the ionic conductivity of the solution. The temperature at which $[Ca(\mu_2\text{-}TFSI)(G4)]^+$ formation occurs can be considered as "critical temperature", which is associated with a decrease in the solution ionic conductivity.

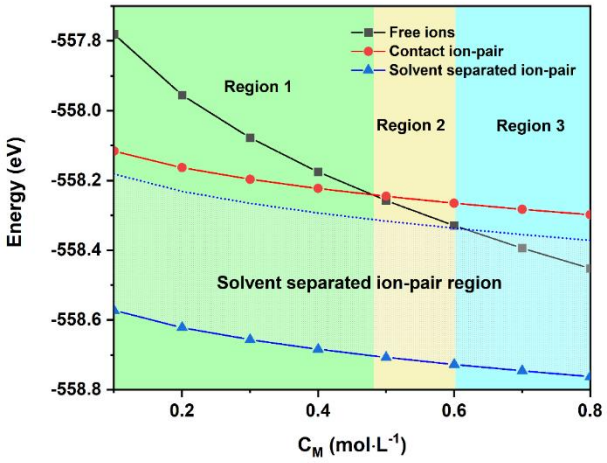

Figure 3. Concentration-dependent free enthalpy of: Free *mer*-$[Ca(G4)_2]^{2+}$ and $TFSI^-$ (Black line), Contact ion-pair *trans*-$[Ca(\mu_2\text{-}TFSI)(G4)]^+$ with a G4 molecule in its second solvation shell (Red

line), and Solvent-separated ion-pair $[[Ca(G4)_2]//TFSI]^+$ (Blue line). The dotted region indicates the energy range of solvent-separated ion-pairs with a consideration of different Ca^{2+} solvation forms. The coloured areas represent different stability domains of the species.

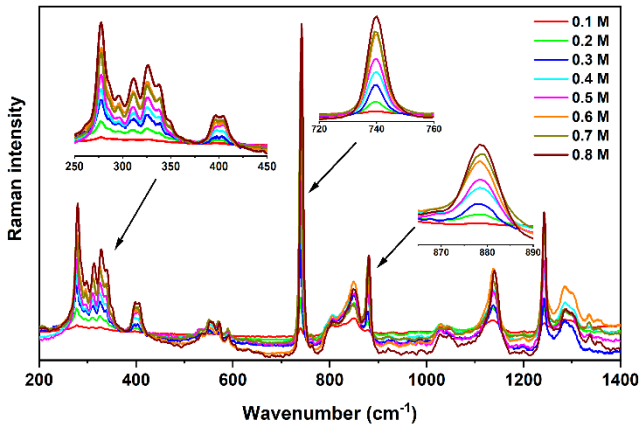

Figure 4. Raman spectra acquired on $Ca(TFSI)_2$/G4 solutions at different salt concentrations. Insets focus on the zoom of some important vibrational modes.

Ion-pair Formation Detection. In order to verify these theoretical predictions, Raman spectroscopy was employed to follow the evolution in the nature of $TFSI^-$ anion upon heating. This technique is capable of distinguishing $TFSI^-$ in the contact ion-pairs from those being in the outer-sphere of Ca^{2+} or free in the solution.

Figure 4 shows the Raman spectra obtained for various $Ca(TFSI)_2$/G4 solutions. The characteristic vibrational modes of $TFSI^-$ and Ca^{2+}/G4 system are: *i*) the symmetric and anti-symmetric SO_2 wagging modes (ω) at 397 and 408 cm^{-1}, *ii*) the symmetric CF_3 bending (δ) coupling with expansion-contraction of O=S–N–S=O group at 740 cm^{-1}, *iii*) the deformation vibration of C–H, C–C, and C–O bonds of G4 molecules coordinated to Ca^{2+} at 868 and 879 cm^{-1}, and *iv*) the C–F stretching mode (ν) at 1242 cm^{-1}.[40] As shown in **Figure 4**, the intensity of these characteristic vibrational modes increases gradually with the salt concentration.

Among all characteristic vibrations, the essential one is the $TFSI^-$ contraction-expansion mode locating at 740 cm^{-1}. It has a trivial intensity in IR spectroscopy but is the most intense band observed in Raman spectroscopy. It is originated from the symmetric CF_3 bending (δ) and the expansion-contraction of the O=S–N–S=O group, the coupling of which could result from the wavenumber superposition or a Fermi resonance (**Video 1**).[40–43] The deconvolution of this signal required at least three components located at: *i*) 731 cm^{-1} to take into account the background effect[41], *ii*) 740 cm^{-1} corresponding to free $TFSI^-$, including those residing in the second coordination sphere of Ca^{2+} in G4 solution (3 cm^{-1} shifted compared to free $TFSI^-$), and *iii*) 748 cm^{-1} corresponding to the $TFSI^-$ coordinated to a M^{n+} in the ion-pair (**Video 2**), i.e. Ca^{2+} in this study (**Figure S9**). Even though the Ca^{2+}–O stretching component in the vibrational eigenvector was relatively weak in this wavenumber range, it was sufficient to modify the force constant and the vibrational wavenumber of the $TFSI^-$ group. Assuming a similar sensitivity to Raman scattering of free and coordinated $TFSI^-$, the Raman intensity ratio reflects the percentage of each kind of $TFSI^-$ that is present in the electrolyte. At a molar concentration greater than 0.3 M, the integrated area of the 748 cm^{-1} band always equals *ca.* 10 % of the total area of the 740 cm^{-1}-centered vibrations (**Table S1**) indicating a nearly constant fraction of ion-pairs in the solution. At lower salt concentrations, i.e. 0.1 M and 0.2 M, the peak at 748 cm^{-1} has a higher contribution (**Table S1**), indicating that $[Ca(\mu_2\text{-}TFSI)(G4)]^+$ ion-pairs are formed and can be observed partially at ambient temperature. This result agrees with theoretical predictions and confirms the presence of free Ca^{2+} and $TFSI^-$ ions at high salt concentrations, consistent with the ionic conductivity of these concentrated solutions at moderated temperatures.

To demonstrate the important presence of contact ion-pairs upon heating, temperature-dependent *in situ* Raman spectroscopy was performed on the solution with the weakest ionic strength, 0.1 M $Ca(TFSI)_2$/G4. The *in situ* experiment was focused especially on the vibrations around 740 cm^{-1} as they can provide quantitative information on the amount of binding and free $TFSI^-$ in the solution. **Figure 5** shows the evolution in intensity of this band as a function of temperature. Upon heating, the intensity of the signal corresponding to free $TFSI^-$ decreases while the one of binding $TFSI^-$ gradually grows (**Figure 5**), indicating a temperature-driven formation of contact ion-pairs. The increasing amount of $[Ca(\mu_2\text{-}TFSI)(G4)]^+$ ion-pair leads to a loss in the number of charge carriers and a change in the mean diffusion coefficient. These phenomena are entirely coherent with the loss in ionic conductivity of the 0.1 M $Ca(TFSI)_2$/G4 solution, the deviation from the VTF-law, and the peculiar behaviour of Walden product at elevated temperatures. By taking into account the presence of free and binding $TFSI^-$, the corrected Walden product shows a constant line in the whole temperature range, which ensured the sole role of ion-pairing in the abnormal behaviour of 0.1 M $Ca(TFSI)_2$/G4 solution (**Figure S10**).

For comparison purpose, Raman measurement was also conducted on a 0.2 M LiTFSI/G4 solution (i.e. same $TFSI^-$ concentration as in 0.1 M $Ca(TFSI)_2$/G4). Results show a gradual decrease in the band's intensity at 740 cm^{-1} when temperature increased (**Figure S11**), which is due to a change in its Raman activity. Nevertheless, the signal of [Li–TFSI] contact ion-pair is not detected in this temperature range. This comparison reveals different solvation and ion-pair structures for mono- and divalent cations, as discussed below.

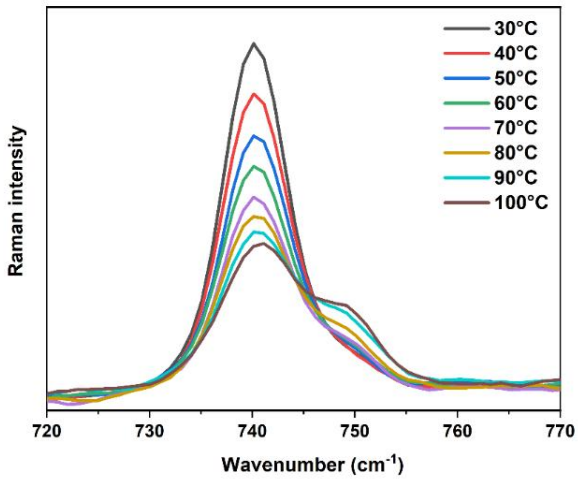

Figure 5. Evolution in the position and the intensity of the characteristic expansion-contraction mode of $TFSI^-$ at 740 cm^{-1} during the temperature-dependent in situ Raman measurement performed on a 0.1 M $Ca(TFSI)_2$/G4 solution.

Discussions

Organic carbonates have long been the focus of battery community as practical solvent for electrolytes in rechargeable LIBs.[44] Nonetheless, carbonate molecules possess a high dipole moment that will be greatly polarised when they are coordinated to a highly charged cation, such as Mg^{2+}, Ca^{2+}, and Al^{3+}. The carbonate molecules in the first coordination sphere of multivalent ions will consequently be reduced before the metal deposition can occur.[13] On the other hand, non-polar solvents, such as glyme molecules, can exhibit great reduction stability even if they are coordinated to a highly polarised cation. Nonetheless, it has long been considered that glyme-based solutions are not ideal electrolytes for batteries as they possess a low dielectric constant and would poorly dissociate the ions. Depending on the chain length, glyme molecules can actually act as multidentate ligands[45], and the solvated ions are highly stabilised through a chelating effect facilitated by the relatively low mechanical stress associated with the glyme strain. Long-chain glyme-based molecules, e.g. triglyme and tetraglyme, can thus dissolve a significant amount of salts, which can be used as electrolytes for rechargeable batteries.[14]

The great influence of the ionic strength on the stability of charged ions is a peculiar property of solvents possessing a low dielectric constant value, in which long-range electrostatic interactions have a great contribution on the system's total energy. In most studies, the theoretical enthalpy or Gibbs free energy of a reaction in liquid phase is computed in a molecular approach (isolated molecules/ions surrounded by an implicit solvent model) that assumes an infinite dilution. Such a consideration is only appropriate when investigating highly dilute solutions in high dielectric constant media, where the ion–ion interaction is completely smeared out. In solutions containing a significant amount of solute, the ion–ion interaction must be included in the total energy by applying the Debye-Hückel solution model[18], only valid in high-dielectric media, as a data post-treatment process. As an alternative of the Debye-Hückel for low dielectric constant media, the present study shows that affordable periodic calculations with varied simulation boxes including punctual counter-ions, e.g. Cl^-, lead to reliable results that qualitatively compare with experimental data.

Based on this methodology, the solvation properties of various concentrated $Ca(TFSI)_2$/G4 solutions were investigated to elucidate the abnormal behaviour experimentally observed for their ionic conductivity. Results show that solvated Ca^{2+} in G4 solutions has a great tendency to form solvent-separated ion-pairs due to the strong electrostatic interaction of Ca^{2+} with the counter $TFSI^-$ ion located in its outer-sphere. At high concentration, free ion *mer*-$[Ca(G4)_2]^{2+}$ is even more stabilised than the solvent-separated species (**Figure 3**) making it the dominant species thanks to the strong ionic strength of the medium allowing long-range electrostatic stabilisation.

Upon heating, both the conductivity and temperature-dependent Raman measurements suggest that solvent-separated ion-pairs or free ions evolve toward $[Ca(\mu_2\text{-}TFSI)(G4)]^+$ contact ion-pairs. Using the energy analysis approach as described in Refs [29,46], the interaction energy of Ca^{2+}–O bonds and strain energy required for the deformation of G4 molecules in free *mer*-$[Ca(G4)_2]^{2+}$ and $[Ca(\mu_2\text{-}TFSI)(G4)]^+$ can be deconvoluted (**Table 1**). The Ca^{2+}–O ($TFSI^-$) interaction energy is 40% stronger than Ca^{2+}–O (G4), i.e. -265 *vs* -185 $kJ{\cdot}mol^{-1}$, due to an enhanced electrostatic interaction between Ca^{2+} and $TFSI^-$, inducing a competition between Ca^{2+}–O ($TFSI^-$) and Ca^{2+}–O (G4). Nonetheless, the number of Ca^{2+}–O bonds being one less in $[Ca(\mu_2\text{-}TFSI)(G4)]^+$ [5+2] than in *mer*-$[Ca(G4)_2]^{2+}$ [4+4], the total Ca^{2+}–O interaction energies in the two systems turn to be very similar (**Table 1**). The direction of the chemical equilibrium between these two species can be easily switched by a small energy variation due to concentration/temperature changes. Moreover, the replacement of a tetraglyme molecule in the doubly-charged *mer*-$[Ca(G4)_2]^{2+}$ complex by $TFSI^-$ leads to a decrease in the ionic strength of the media together with a significant increase in the system's entropy due to the multiple configurations of a free tetraglyme molecule. These two factors are the driving force for the contact ion-pair formation upon heating, which fully rationalises the decrease in the ionic conductivity with temperature.

Overall, the results presented in this study demonstrate a subtle chemical equilibrium existing in $Ca(TFSI)_2$/G4 solution between solvated Ca^{2+} and singly-charged ion-pairs (solvent-separated or contact). The weakly endergonic reaction enthalpy computed at 0K for the $[Ca(G4)_2]^{2+} + TFSI^- \rightleftharpoons [Ca(\mu_2\text{-}TFSI)(G4)]^+ + G4$ equilibrium is sufficient to explain why $Ca(TFSI)_2$/G4 solutions are so sensitive to concentration and/or temperature effects. Whether this equilibrium turns in favour of ion-pair association or dissociation clearly lies in the enthalpy/entropy competition one may tune through the modulation of concentration and temperature. Increasing salt concentration moves the equilibrium towards ion-pair dissociation thanks to the ionic strength (enthalpy gain) which stabilises solvated Ca^{2+} above a critical concentration (Region 2). While this is beneficial to ionic conductivity, the persistent occurrence of solvent-separated ion-pairs, irrespectively of the concentration, contributes to reduce the optimal ionic conductivity one may envision in solutions with solely solvated Ca^{2+}. One way to prevent the dominant contribution of solvent-separated ion-pairs at low salt concentrations would be to monitor the solution's ionic strength through the so-called "salt effect". As an example, adding non-electroactive salts, such as $[N(Bu)_4]Cl$, would increase the ionic strength of the solution and favour fully solvated *mer*-$[Ca(G4)_2]^{2+}$ species even at low $Ca(TFSI)_2$ concentrations.

Increasing the temperature now moves the equilibrium towards ion-pair association thanks to the entropy gain associated with the conversion of Ca-chelating G4 having a few accessible conformations, into free G4 having around 3^{14} accessible conformations. Remarkably, temperature does not act as a stabiliser of contact ion-pair but triggers its formation indirectly from the large entropy gain associated with the increasing fraction of free tetraglymes in the solution. The detrimental impact of ion-pairing on the ionic conductivity of the solution could be easily prevented by using longer-chains glyme solvents up to polyethylene oxide (PEO) polymers. Indeed, while the enthalpy contribution to

the solvation structures of Ca^{2+} is expected to be similar in $Ca(TFSI)_2$/PEO polymer electrolytes and in liquid ethereal solutions, the important loss in configuration entropy in longer-chains free glymes and polymers should prevent or delay the formation of ion-pairs towards higher temperatures. Therefore, $Ca(TFSI)_2$/PEO is expected not to be a strong entropy-driven system as tetraglyme and its properties should be mainly dictated by ionic strength making it a better ionic conductor than liquid $Ca(TFSI)_2$/G4.

At this stage, one may wonder whether the peculiar behaviour observed in $Ca(TFSI)_2$/G4 will also be encountered in other systems, such as $Mg(TFSI)_2$/G4 solutions. In order to clarify this point, a 0.5 M $Mg(TFSI)_2$/G4 solution was prepared, and its temperature-dependence conductivity was also measured (**Figure 6a**). The $\sigma = f(\frac{1}{T})$ relation also shows a non-monotonic response: there exists a "critical" temperature, beyond which the solution conductivity starts to deviate from the VTF model, alike in $Ca(TFSI)_2$/G4 solutions. This phenomenon is also assigned to the ion-pair formation at elevated temperatures. In a recent study, we have demonstrated that Mg^{2+} in G4 solution shows structural flexibility. In G4-deficient conditions, Mg^{2+} exists in the form of $[Mg(G4)]^{2+}$ while two G4 molecules participate in the solvation process to generate *mer*-$[Mg(G4)_2]^{2+}$ [3+3] when there is a G4 surplus.[29] In 0.5 M $Mg(TFSI)_2$/G4 solution, *mer*-$[Mg(G4)_2]^{2+}$ is the preferred solvation form and the $[Mg(TFSI)(G4)]^+$ ion-pair formation reaction can be written as in **Figure S12**. Nevertheless, there is a transformation in the coordination number of Mg^{2+} from [3+3] to [5+2] during the ion-pair association (**Figure S12**). Alike Ca^{2+}, Mg^{2+} ion-pair can exist in the form $[Mg(\mu_1\text{-TFSI})(G4)]^+$ or $[Mg(\mu_2\text{-TFSI})(G4)]^+$ with the latter being more stable (**Figure 6b**). The thermodynamic properties of ion-pair formation in 0.5 M $Mg(TFSI)_2$/G4 solution is then expected to be similar as in $Ca(TFSI)_2$/G4 solutions, therefore favouring the $[Mg(\mu_2\text{-TFSI})(G4)]^+$ formation at elevated temperatures. These findings are consistent with previous studies showing that in low-permittivity solvents, such as monoglyme, diglyme, or triglyme, the fraction of free Mg^{2+} in $Mg(TFSI)_2$-based electrolytes increases at higher salt concentrations.[47–50] **Table S2** summarises the Mg^{2+}–O interaction energy with different glymes, from monoglyme up to tetraglyme; it is apparent that the strength of Mg^{2+}–O interaction is invariant with the chain length. Moreover, all glyme-based media exhibit similar dielectric constant (ε_r = 7.2−7.5). The invariance in the magnitude of the short- and long-range interactions when varying the chain length is the origin of the abnormalities observed in glyme-based solutions containing divalent salts. The physical properties of low dielectric $Mg(TFSI)_2$/G4 and $Ca(TFSI)_2$/G4 solutions are thus very different from those known for conventional electrolytes. Therefore, suitable ionic strength must be tuned through the "salt effect" when employing $Mg(TFSI)_2$/G4 or $Ca(TFSI)_2$/G4 as electrolyte for rechargeable batteries in order to maximise the amount of free solvated ions.

These findings now allow us to rationalise the different behaviour of LiTFSI/G4 system, where no ion-paring is detected in 0.2 M solution even at elevated temperatures (**Figure S11**). According to our previous study, Li^+ in G4 solution is solvated in the $[Li(G4)]^+$ form with all five oxygen atoms of the G4 molecule participate in the coordination.[29,51] The ion-pairing reaction, $[Li(G4)]^+ + TFSI^- \rightleftharpoons [Li(TFSI)(G4)]$ is now associated with a loss in entropy due to the combination of ions, which cannot occur at high temperatures. Furthermore, $[Li(G4)]^+$ bears one charge and is stabilised at all concentrations due to the ionic strength, which is not the case for the [Li(TFSI)(G4)] neutral species. In LiTFSI/G4 solutions, both enthalpic and entropic effects tend to favour the existence of solvated $[Li(G4)]^+$, irrespective of the concentration and temperature.

In this study, the leading parameters governing the solvation properties of generic $M^{n+}(TFSI)_n$/Gm solutions were identified and their associated ionic conductivity fully rationalised. These factors should be listed as follows:

- Short-range chemical interactions: they are determined by the strength of the interaction between the solvated cation and the solvent molecules in the first solvation sphere and their magnitude is proportional to Z^2, Z being the charge of the central ion.
- Long-range electrostatic interactions: they are dominant in low-dielectric media and their magnitude is proportional to the charge of the solvated species present in the solution.
- Solvent configuration entropy: this quantity is critical for solvents undergoing large entropy variation during the (de)solvation process.
- Solvent stress: this quantity is indirectly linked to the previous one and is related to the strain energy required for a solvent molecule to coordinate to the central ion. It is negligible in monodentate ligands/solvent molecules but might become important in some multidentate ligands when electron-donor atoms need to drastically reorganise to coordinate the central cations. As a destabilizing factor competing with the solvation energy, it can prevent the separation of anions and cations.

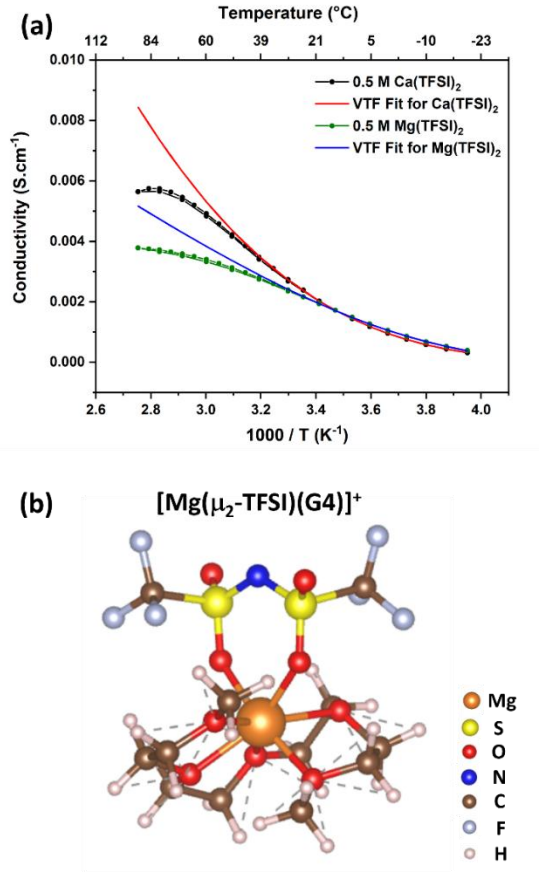

Figure 6. (a) Temperature dependence of the conductivity of 0.5 M $Mg(TFSI)_2$/G4 solution compared to 0.5 M $Ca(TFSI)_2$/G4. A divergence from the VTF model was observed for both solutions. (b) Structure of $[Mg(\mu_2\text{-TFSI})(G4)]^+$ ion-pair optimised by the SCAN-rVV10 functional embedded in the VASP code.

Table 1. Energy of M–O bonds in *mer*-$[Ca(G4)_2]^{2+}$ and $[Ca(\mu_2\text{-TFSI})(G4)]^+$, and the energy required for the G4 deformation calculated with the SCAN-rVV10 functional in the VASP code. The coordination number of each central ion is indicated in square brackets. All calculations were performed using the simulation box in the size of 20 × 20 × 20 Å.

	Total M–O energy ($kJ{\cdot}mol^{-1}$)	Average energy per M–O bond ($kJ{\cdot}mol^{-1}$)	Energy per M–O (TFSI) bond ($kJ{\cdot}mol^{-1}$)	Strain energy for G4 ($kJ{\cdot}mol^{-1}$)	Percentage of G4 strain energy compared to M–O energy
***mer*-$[Ca(G4)_2]^{2+}$ [4+4]**	-1463.0	-182.9		97.5	6.7%
$[Ca(\mu_2\text{-TFSI})(G4)]^+$ [5+2]	-1444.7	-206.4	-265.2	48.2	3.3%

The above-mentioned factors exist in all kinds of liquid electrolytes at different extents, influencing the stability and the reactivity of the solvated cations. In conventional carbonate-based electrolytes, the dielectric constant is usually quite large and the organic carbonate molecules are monodentate[52–56], so that their solvation properties are primarily dominated by the short-range chemical interactions. In tetraglyme solvent, the G4 molecule is multidentate with five electron-donor oxygens and the chelation occurs due to a moderate solvent stress. Therefore, these intermediate molecular weight glyme-based systems should be considered as "entropy-driven solvents". Due to its low dielectric constant, the long-range electrostatic interaction is not negligible, which can directly affect the energy of the solvated ions. Nevertheless, the low-dielectric medium opens the possibility to modulate the solvent properties, such as the structure and the solvation energy, through a variation of the ionic strength at different solution concentrations, which might have a paramount impact on the interface stability and the reactivity of the solvated species.

Besides electrochemistry, several biochemical processes, such as enzyme activations or protein–inhibitor interaction, have been reported to occur in extremely low dielectric constant environments with the peculiar role of the ion-pairing process.[57–59] Consequently, the results and methodology developed in this study can further be applied to these systems.

Conclusions

In this study, we have investigated the particular conductivity behaviour of $Ca(TFSI)_2$/G4 and $Mg(TFSI)_2$/G4 solutions *vs* concentration and temperature. For weak ionic force solutions, solvent-separated ion-pair is the most energetically favourable species and upon heating, a critical temperature exists, beyond which the ion-pair formation occurs, thus driving the ionic conductivity down and leading to a change of the Walden product with temperature. In high concentration solutions, the free solvated ions become favoured thanks to the high ionic strength of the solution. These behaviours are completely different from those observed in conventional carbonate-based electrolytes and in LiTFSI/G4 electrolytes, which is a consequence of the low-dielectric medium with divalent cations (in contrast to monovalent) and the high configuration entropy change coming from the release of multidentate flexible G4 molecules. These unexpected behaviours can be explained using periodic electrolyte models in which explicit solvated species are surrounded in an implicit solvent model and where the boundary conditions can be used to vary the salt concentration. This approach allows capturing the long-range electrostatic interactions and their influence on the energy of the different solvated species expected to occur in the solutions. The present analysis not only rationalises the abnormal ionic conductivity behaviour of $[M^{2+}(TFSI^-)_2]$/G4 solutions but also sheds light on the three leading parameters that can be tuned to design better electrolytes: ionic strength, solvent conformational entropy, and solvation stress. These findings, hopefully, will lead to a paradigm shift in how solvated ions and molecular electrolytes are modelled, which might impact the development of new electrolytes, especially those for multivalent rechargeable batteries as well as electrolysis and electrocatalysis.

Author Contributions

L.H.B.N. conducted the DFT calculations, interpreted the data, and wrote the manuscript. T.P. carried out the sample preparation and experimental measurement L.H.B.N. and T.P. contributed equally to this work. N. S. developed the *in situ* Raman apparatus and helped with the vibrational spectroscopy data treatment. C. I. and F. A. designed and helped with experimental data treatment and supervised the experimental work. M-L.D. and J-S.F. developed the theoretical framework and supervised the theoretical work. All the authors discussed the results and edited the manuscript.

Conflicts of interest

There are no conflicts to declare.

Acknowledgements

This research work has been founded by the European FET-Open project VIDICAT (Grant Agreement: 829145). This work was performed using HPC resources from GENCI-CINES (grant 2020-A0080910369). The authors acknowledge Vincent Verdoot (Université Grenoble Alpes, Laboratoire de Rhéologie et Procédés,

F-38000 Grenoble, France) for his helps with the rheology measurements. L.H.B.N., M.-L.D., and J.-S.F. thank the French National Research Agency (STORE-EX Labex project ANR-10LABX-76-01) for financial support.

References

1 M. Armand and J.-M. Tarascon, *Nature*, 2008, **451**, 652–657.

2 D. Larcher and J.-M. Tarascon, *Nat. Chem.*, 2015, **7**, 19–29.

3 R. B. Kaunda, *J. Energy Nat. Resour. Law*, 2020, **38**, 237–244.

4 D. B. Agusdinata, W. Liu, H. Eakin and H. Romero, *Environ. Res. Lett.*, 2018, **13**, 123001.

5 C. Banza Lubaba Nkulu, L. Casas, V. Haufroid, T. De Putter, N. D. Saenen, T. Kayembe-Kitenge, P. Musa Obadia, D. Kyanika Wa Mukoma, J. M. Lunda Ilunga, T. S. Nawrot, O. Luboya Numbi, E. Smolders and B. Nemery, *Nat. Sustain.*, 2018, **1**, 495–504.

6 A. Ponrouch, J. Bitenc, R. Dominko, N. Lindahl, P. Johansson and M. R. Palacin, *Energy Storage Mater.*, 2019, **20**, 253–262.

7 Y. Tian, G. Zeng, A. Rutt, T. Shi, H. Kim, J. Wang, J. Koettgen, Y. Sun, B. Ouyang, T. Chen, Z. Lun, Z. Rong, K. Persson and G. Ceder, *Chem. Rev.*, 2021, **121**, 1623–1669.

8 A. Ponrouch and M. R. Palacin, *Curr. Opin. Electrochem.*, 2018, **9**, 1–7.

9 M. E. Arroyo-de Dompablo, A. Ponrouch, P. Johansson and M. R. Palacín, *Chem. Rev.*, 2020, **120**, 6331–6357.

10 J. B. Goodenough and K.-S. Park, *J. Am. Chem. Soc.*, 2013, **135**, 1167–1176.

11 J. B. Goodenough and Y. Kim, *Chem. Mater.*, 2010, **22**, 587–603.

12 K. Xu, *Chem. Rev.*, 2004, **104**, 4303–4417.

13 A. Kopač Lautar, J. Bitenc, T. Rejec, R. Dominko, J. S. Filhol and M. L. Doublet, *J. Am. Chem. Soc.*, 2020, **142**, 5146–5153.

14 N. T. Hahn, S. A. McClary, A. T. Landers and K. R. Zavadil, *J. Phys. Chem. C*, 2022, **126**, 10335–10345.

15 D. M. Driscoll, N. K. Dandu, N. T. Hahn, T. J. Seguin, K. A. Persson, K. R. Zavadil, L. A. Curtiss and M. Balasubramanian, *J. Electrochem. Soc.*, 2020, **167**, 160512.

16 N. T. Hahn, D. M. Driscoll, Z. Yu, G. E. Sterbinsky, L. Cheng, M. Balasubramanian and K. R. Zavadil, *ACS Appl. Energy Mater.*, 2020, **3**, 8437–8447.

17 A. M. Melemed, D. A. Skiba and B. M. Gallant, *J. Phys. Chem. C*, 2022, **126**, 892–902.

18 Y. Marcus and G. Hefter, *Chem. Rev.*, 2006, **106**, 4585–4621.

19 S. Terada, T. Mandai, S. Suzuki, S. Tsuzuki, K. Watanabe, Y. Kamei, K. Ueno, K. Dokko and M. Watanabe, *J. Phys. Chem. C*, 2016, **120**, 1353–1365.

20 J.-L. Souquet, M. L. F. Nascimento and A. C. M. Rodrigues, *J. Chem. Phys.*, 2010, **132**, 034704.

21 J. L. Souquet, in *Defects and Disorder in Crystalline and Amorphous Solids*, Springer Netherlands, Dordrecht, 1994, pp. 221–244.

22 S. B. Aziz, T. J. Woo, M. F. Z. Kadir and H. M. Ahmed, *J. Sci. Adv. Mater. Devices*, 2018, **3**, 1–17.

23 J. D. Forero-Saboya, E. Marchante, R. B. Araujo, D. Monti, P. Johansson and A. Ponrouch, *J. Phys. Chem. C*, 2019, **123**, 29524–29532.

24 T. M. Pappenfus, W. A. Henderson, B. B. Owens, K. R. Mann and W. H. Smyrl, *J. Electrochem. Soc.*, 2004, **151**, A209.

25 D. Brouillette, D. E. Irish, N. J. Taylor, G. Perron, M. Odziemkowski and J. E. Desnoyers, *Phys. Chem. Chem. Phys.*, 2002, **4**, 6063–6071.

26 M. Nakahara and K. Ibuki, *J. Phys. Chem.*, 1986, **90**, 3026–3030.

27 D. R. MacFarlane, M. Forsyth, E. I. Izgorodina, A. P. Abbott, G. Annat and K. Fraser, *Phys. Chem. Chem. Phys.*, 2009, **11**, 4962–4967.

28 C. T. Moynihan, *ECS Proc. Vol.*, 1981, **1981–10**, 256–274.

29 L. H. B. Nguyen, T. Picard, N. Sergent, C. Raynaud, J.-S. Filhol and M.-L. Doublet, *Phys. Chem. Chem. Phys.*, 2021, **23**, 26120–26129.

30 L. Xue, D. D. DesMarteau and W. T. Pennington, *Solid State Sci.*, 2005, **7**, 311–318.

31 L. Xue, C. W. Padgett, D. D. DesMarteau and W. T. Pennington, *Solid State Sci.*, 2002, **4**, 1535–1545.

32 S. Tsuzuki, T. Mandai, S. Suzuki, W. Shinoda, T. Nakamura, T. Morishita, K. Ueno, S. Seki, Y. Umebayashi, K. Dokko and M. Watanabe, *Phys. Chem. Chem. Phys.*, 2017, **19**, 18262–18272.

33 P. Johansson and P. Jacobsson, *J. Phys. Chem. A*, 2001, **105**, 8504–8509.

34 K. Hashimoto, S. Suzuki, M. L. Thomas, T. Mandai, S. Tsuzuki, K. Dokko and M. Watanabe, *Phys. Chem. Chem. Phys.*, 2018, **20**, 7998–8007.

35 S. H. Lapidus, N. N. Rajput, X. Qu, K. W. Chapman, K. A. Persson and P. J. Chupas, *Phys. Chem. Chem. Phys.*, 2014, **16**, 21941–21945.

36 N. N. Rajput, T. J. Seguin, B. M. Wood, X. Qu and K. A. Persson, *Elucidating Solvation Structures for Rational Design of Multivalent Electrolytes—A Review*, Springer International Publishing, 2018, vol. 376.

37 N. N. Rajput, X. Qu, N. Sa, A. K. Burrell and K. A. Persson, *J. Am. Chem. Soc.*, 2015, **137**, 3411–3420.

38 G. A. Giffin, A. Moretti, S. Jeong and S. Passerini, *J. Phys. Chem. C*, 2014, **118**, 9966–9973.

39 N. T. Hahn, J. Self, D. M. Driscoll, N. Dandu, K. S. Han, V. Murugesan, K. T. Mueller, L. A. Curtiss, M. Balasubramanian, K. A. Persson and K. R. Zavadil, *Phys. Chem. Chem. Phys.*, 2022, **24**, 674–686.

40 I. Rey, P. Johansson, J. Lindgren, J. C. Lassègues, J. Grondin and L. Servant, *J. Phys. Chem. A*, 1998, **102**, 3249–3258.

41 L. Aguilera, S. Xiong, J. Scheers and A. Matic, *J. Mol. Liq.*, 2015, **210**, 238–242.

42 M. Herstedt, M. Smirnov, P. Johansson, M. Chami, J. Grondin, L. Servant and J. C. Lassègues, *J. Raman Spectrosc.*, 2005, **36**, 762–770.

43 L. Edman, *J. Phys. Chem. B*, 2000, **104**, 7254–7258.

44 K. Xu, *Chem. Rev.*, 2014, **114**, 11503–11618.

45 R. Andersson, G. Hernández and J. Mindemark, *Phys. Chem. Chem. Phys.*, 2022, 499–523.

46 P. Johansson, J. Tegenfeldt and J. Lindgren, *Polymer (Guildf).*, 1999, **40**, 4399–4406.

47 N. Sa, N. N. Rajput, H. Wang, B. Key, M. Ferrandon, V. Srinivasan, K. A. Persson, A. K. Burrell and J. T. Vaughey, *RSC Adv.*, 2016, **6**, 113663–113670.

48 M. Salama, I. Shterenberg, H. Gizbar, N. N. Eliaz, M. Kosa, K. Keinan-Adamsky, M. Afri, L. J. W. Shimon, H. E. Gottlieb, D. T. Major, Y. Gofer and D. Aurbach, *J. Phys. Chem. C*, 2016, **120**, 19586–19594.

49 J. Self, N. T. Hahn, K. D. Fong, S. A. McClary, K. R. Zavadil and K. A. Persson, *J. Phys. Chem. Lett.*, 2020, **11**, 2046–2052.

50 T. Kimura, K. Fujii, Y. Sato, M. Morita and N. Yoshimoto, *J. Phys. Chem. C*, 2015, **119**, 18911–18917.
51 S. Saito, H. Watanabe, Y. Hayashi, M. Matsugami, S. Tsuzuki, S. Seki, J. N. Canongia Lopes, R. Atkin, K. Ueno, K. Dokko, M. Watanabe, Y. Kameda and Y. Umebayashi, *J. Phys. Chem. Lett.*, 2016, **7**, 2832–2837.
52 J. C. Soetens, C. Millot and B. Maigret, *J. Phys. Chem. A*, 1998, **102**, 1055–1061.
53 M. D. Bhatt, M. Cho and K. Cho, *Appl. Surf. Sci.*, 2010, **257**, 1463–1468.
54 V. Ponnuchamy, S. Mossa and I. Skarmoutsos, *J. Phys. Chem. C*, 2018, **122**, 25930–25939.
55 K. Tasaki, A. Goldberg and M. Winter, *Electrochim. Acta*, 2011, **56**, 10424–10435.
56 M. G. Giorgini, K. Futamatagawa, H. Torii, M. Musso and S. Cerini, *J. Phys. Chem. Lett.*, 2015, **6**, 3296–3302.
57 E. L. Mertz and L. I. Krishtalik, *Proc. Natl. Acad. Sci. U. S. A.*, 2000, **97**, 2081–2086.
58 L. I. Krishtalik, *Photosynth. Res.*, 1999, **60**, 241–246.
59 Y. Li, Y. Cong, G. Feng, S. Zhong, J. Z. H. Zhang, H. Sun and L. Duan, *Struct. Dyn.*, , DOI:10.1063/1.5058172.

